Reactive Atmosphere Synthesis of Polymer-derived Si-O-C-N Aerogels and their Cr Adsorption from Aqueous Solutions

E. Zera, E. Brancaccio, L. Tognana, L. Rivoira, M. C. Bruzzoniti, G. D. Sorarù

Reactive Atmosphere Synthesis of Polymer-derived Si-O-C-N Aerogels and their Cr Adsorption from Aqueous Solutions

Advanced Engineering Materials

2018, 10.1002/adem.201701130

Reactive Atmosphere Synthesis of Polymer-derived Si-O-C-N Aerogels and their Cr Adsorption from Aqueous Solutions

E. Zera[1,3], E. Brancaccio[1], L. Tognana[1], L. Rivoira[2], M. C. Bruzzoniti[2], G. D. Sorarù[3]

1 Solidpower SpA, Via Trento, 115/117, 38017, Mezzolombardo, Trento, Italy
2 Dipartimento di Chimica, Università di Torino
3 Dipartimento di Ingegneria Industriale, Via Sommarive 9, 38123 Trento, Italy

Abstract

Polymer derived ceramic (PDCs) aerogels belonging to the Si-O-C-N system were synthesized by crosslinking a preceramic polymer in a diluted solution followed by supercritical or atmospheric drying and pyrolysis in inert (N_2) or reactive (NH_3/CO_2) atmosphere. Accordingly, aerogels with hierarchical porosity ranging from some microns to few nanometers together with high specific surface area in the range 30 - 400 m^2/g have been obtained. Moreover, their surface contains a broad range of moieties (Si-OH, Si-NH, C=O, etc.) that could interact and bind metal ions thanks to electrostatic interactions. This combination of hierarchical porosity, high SSA and broad range of chemical functionalities makes these PDCs aerogels interesting candidates for water purification. In this work SiOC and SiCN aerogels have been tested as adsorbents for Cr(III)/(VI) ions from aqueous solutions with promising results for the SiOC aerogel pyrolyzed in N_2 and the SiCN treated in NH_3. Correlations and similarities among the Cr(VI)/(III) adsorption capacity with the main features of the porous substrates (SSA, N_2 TPV, amount of free C, bulk density, isoelectric point, main IR peaks (Si-OH, OH, NH, C=O, C=C, Si-O, C-N, Si-N) have been investigated by applying the Principal Component Analysis (PCA).

1. Introduction

High-temperature Si-based ceramics obtained by pyrolysis of preceramic polymers (PDCs), have shown, together with creep resistance to very high temperature, other interesting electrical/electrochemical and optical properties [1, 2, 3, 4]. More recently, new PDCs processing techniques have been developed ranging from flash pyrolysis -to fabricate ceramic matrix composites (CMC) - to stereolitography -to process ceramic microcomponents- to aerogel synthesis which allows preparing porous components with high surface area and hierarchical porosity [5, 6, 7, 8].

The structure of PDCs is based on two nano-sized interpenetrating phases, one formed by an amorphous network containing Si-C, Si-O and Si-N bonds and the other one consisting of sp^2 C layers organized as turbostratic carbon [9]. The nature of the chemical bonds forming the amorphous phase can be controlled either by selecting the suitable pre-ceramic precursor or by using a reactive atmosphere [1]. For example, starting from a polysiloxane different ceramics can be obtained: silicon oxycarbides, SiOCs, whose amorphous network is built up by mixed Si units sharing Si-O and Si-C bonds, can be produced under inert gas (N_2 or Ar) [10], silicon oxynitrides, SiONs, containing Si-O and Si-N bonds are formed in flowing reactive NH_3 [11] and finally a mixture of SiO_2 and C – without any mixed silicon units- is formed under flowing CO_2 [12].

Purification of wastewater from toxic metal ions still represents a challenge. For its widespread use in industrial processes (e.g. tannery, metal plating) chromium is one of the most studied metals for water remediation. In water solution, Cr exists in two oxidation states (trivalent or hexavalent) of different toxicity and bioaccessibility [13]. One of the most popular method in the purification of wastewater containing Cr metal species is based on adsorption on highly porous substrates such as metal oxides or carbons-based materials [14, 15, 16]. These materials contain on their surface native functional groups suitable to bind and/or interact with the metal ion. In some cases, in order to improve the removal efficiency, selected chemical groups can also be grafted on the adsorber surfaces. Only few studies have been reported in the literature concerning the use of PDCs as substrates for water purification [17, 18, 19, 20, 21]. Moreover, in all these works, only the adsorption of organic pollutants was investigated and to the best of our knowledge the removal of metal ions using porous PDCs was just briefly attempted in one recent study [22]. However, PDCs, having a duplex nanostructure containing an inorganic Si-O-C-N network and turbostratic carbon, could offer an interesting new adsorbing material by combining the unique features of the two most studied porous substrates, namely the porous ceramic and the active carbons. Accordingly, in this study, we tested some Si-based, polymer-derived ceramics aerogels belonging to the Si-O-C-N system in the belief that the combination of high SSA and hierarchical porosity (supplied by the aerogel *micro*structure) and wide range of surface moieties (resulting from the PDC structure) could be beneficial to the adsorption of metal ions typically present in industrial wastewater, such as Cr. Moreover, in this study, the composition of the PDCs aerogels has been modified either by changing the starting pre-ceramic polymer or by modifying the pyrolysis atmosphere.

2. Experimental

2.1 Materials preparation

Polymer derived ceramics aerogels were prepared taking advantage of the concept and recipes published in [23]. In particular we focused on SiOC and SiCN composition, so we used an Si-H bearing polysiloxane, namely a poly(methylhydridosiloxane) (PMHS, MW = 1900, CAS: 63148-57-2, Gelest, Morrisville, PA, USA) and a polysilazane (Durazane 1800, CAS: 503590-70-3, Merck, Darmstadt, Germany), we crosslinked them with divinylbenzene (DVB, CAS: 1321-74-0, Sigma-Aldrich, St. Louis, MO, USA) by means of Pt catalyzed hydrosilylation reaction (Karstedt's catalyst, CAS: 68478-92-2, Sigma-Aldrich, St. Louis, MO, USA) in highly diluted conditions and dried them with supercritical CO_2. In the case of the silazane-derived gels, the possibility to maintain the high porosity and high SSA by simple evaporative drying was demonstrated and, for this composition, the CO_2 route was excluded. In details, the polysiloxane aerogels were produced by mixing 1.0 g of PMHS, 2.0 g of DVB, 10.0 g of acetone and 24 µL of 2%Pt Karstedt's catalyst. The solution was sealed in a PTFE lined autoclave (4749 General Purpose Vessel, Parr Instrument) and treated at 150 °C for 6 hours. The formed gels were removed from the autoclave, washed with fresh solvent twice a day for 2 days and loaded in a home built supercritical drier. The initial acetone was exchanged with liquid CO_2 (15 °C, 50 bar) twice a day for 5 days and finally the CO_2 was brought in supercritical condition (45 °C, 100 bar) by heating the supercritical drier with a thermobath. The CO_2 was removed by slow depressurization (rate below 1 bar/min) and the polysiloxane aerogels were removed once the relative pressure reached zero. The polysilazane aerogels were produced by mixing 2.5 g of Durazane 1800, 1.5 g of DVB, 7.9 g of cyclohexane and 20 µL of 2%Pt Karstedt'scatalyst. The solution was treated at 150°C for 20h in the PTFE lined autoclave; the gels were washed with fresh solvent twice a day for 2 days and finally the solvent was allowed to evaporate slowly under the hood over the course of 3 days. The pyrolysis was performed in a tubular furnace equipped with an alumina tube (LindberghBlue) when the atmosphere used was N_2 or CO_2 while a fused quartz tubular furnace (Hearaus) was used for the pyrolysis under ammonia flow. The tube

was purged for 5 hours with N_2 before starting the treatment to remove oxygen traces; the purging and working flow was 300 mL/min, the heating rate 5 °C/min and time at set temperature 2 h. The furnace was cooled at 10 °C/min in N_2 flow. In **Table 1** a summary of the produced samples and the corresponding labels is presented.

Table 1. Summary of the studied samples and their synthesis details (atmosphere and maximum pyrolysis temperature).

Sample	SiOC-N_2	SiOC-CO_2	SiOC-NH_3	SiCN-900	SiCN-1300	SiCN-NH_3
Atmosphere	N_2	CO_2	NH_3	N_2	N_2	NH_3
Temperature (°C)	900	900	900	900	1300	900

2.2 Materials characterization

Pore size distribution and specific surface area (SSA) were measured by nitrogen physisorption with an ASAP 2010 Micromeritics instrument. SSA value was evaluated by multipoint BET method in the p/p_0 range 0.05-0.30, while pore size distribution was computed following the Barrett–Joyner–Halenda (BJH) method from the desorption branch of the isotherms [24]. Chemical bonds were studied with FT-IR (Varian 4100 spectrometer) in transmission mode using the KBr pellet technique acquiring 64 scan with a resolution of 4 cm^{-1}. TG/DSC was performed with a TA instrument STD Q600 in synthetic air flow (100 mL/min) to evaluate the oxidation behavior and the amount of free carbon in the aerogels. The heating rate was 20 °C/min up to 1000°C. The isoelectric point was estimated by dropping 100 mg of aerogel in 10 mL of deionized water (conductivity <0.2 µS/cm) and measuring the pH reached after 1 day with a Crison 2001 pH meter. The SiOC aerogels were also analyzed by ^{29}Si MAS NMR. ^{29}Si Solid state NMR analyses were carried out with a Bruker 300WB instrument operating at a proton frequency of 300.13 MHz. NMR spectra were acquired with SP pulse sequence under the following conditions: ^{29}Si frequency: 59.60 MHz, π/4 pulse length: 2.25 µs, recycle delay: 150 s, 4k scans. Samples were packed in 4 mm zirconia rotors, which were spun at 5 kHz under air flow. Q8M8 was used as external secondary reference.

2.3 Metal ion removal test

Cr adsorption was measured by contacting 30 mg of aerogel with 50 mL of water containing 5, 10, 20, 50, 200 ppm of Cr ions for 1 h. The contaminated water was buffered at pH 5.0 by a 25 mM acetate buffer. One mL of water was sampled, diluted 1:10 with deionized water and analyzed with ICP-OES (SPECTRO Analytical Instruments) to measure the concentration of remaining Cr and calculate the adsorbed amount. Both Cr(VI) and Cr(III) were tested, using K_2CrO_4 and $CrCl_3{\cdot}6H_2O$ salts as source of chromium ions. For the two most promising samples the adsorption kinetic was also measured. Accordingly, 30 mg of aerogel were added to 50 mL of water containing 200 ppm of Cr buffered at pH 5.0 by a 25 mM acetate buffer, sampling 100 µL of water for every time point and diluting it to 10 mL for the ICP measurement. In all the tests the aerogel samples were ground and sieved to obtain coarse powders with size between 200 and 1000 µm.

3. Results and discussion

3.1 Structural and microstructural characterization

When dealing with aerogels the first properties usually measured are the bulk density, the pore size distribution and the specific surface area (SSA). In **Figure 1** the N_2 physisorption isotherms of the SiOC and SiCN aerogels pyrolized in different conditions are shown together with the cumulative pore size distribution curves. Their density, SSA and total pore volume are summarized in **Table 2**. The adsorption/desorption isotherms recorded for the SiOC samples (**Fig. 1a**) are typical Type IV isotherms due to mesoporous materials. For the SiOC samples pyrolyzed in N_2 or NH_3 the hysteresis loop is shifted to higher P/P_0 values compared to the CO_2-pyrolyzed aerogel revealing the formation, for the latter sample, of smaller mesopores. Indeed, pyrolysis in CO_2 flow strongly impact on the aerogel microstructure: (i) the TPV is reduced to ca. 1/2 compared to that of the SiOCs pyrolyzed in N_2 and NH_3 (see **Table 2**); (ii) the mesopore size is reduced from 10 - 30 nm as measured for the N_2 and NH_3 pyrolyzed samples to 8 -15 nm for the CO_2 treated aerogel (**See Fig. 1b**). Moreover, pyrolysis in CO_2 creates also some micropores, as evident by the isotherm which shows a higher pore volume at P/P_0 below 0.05. Micropores are probably formed through the partial removal of the free carbon by the CO_2 as occurs in the common carbon activation process. Moreover, since CO_2 –as will be shown later from the NMR study- is also promoting the cleavage of the Si-C bonds with formation of SiO_2 and C [12, 25] the incipient sintering of the silica matrix could be responsible for the partial consumption of the mesopores volume.

The N_2 isotherms and the cumulative pore size distribution curves reported in **Figures 1 c & d**, reveal that the ambient dried SiCN samples still maintain a certain amount of mesopores and high SSA (**Table 2**), confirming the possibility to obtain an aerogel-like microstructure with a simpler drying procedure, avoiding the SC drying step. This encouraging result prompted us to evaluate if a similar procedure (ambient-drying) could also be applied to the siloxane-derived samples. Accordingly, many recipes of polysiloxane gels with different amount of solvent, catalyst and crosslinking time were synthesized but none of them allowed maintaining the porous structure with conventional evaporative drying.
Pyrolysis in ammonia deeply affects the microstructure of SiCN samples by creating micro and mesopores that contribute to decrease the density and increase SSA and TPV. The mechanism explaining the effect of ammonia on increasing the porosity of the resulting aerogel is rather complex and it goes beyond the scope of this study however we could tentatively ascribe the formation of micropores and small mesopores to the consumption of part of the carbon by the molecular hydrogen produced by the high temperature decomposition of ammonia [26]. A microstructural evolution is observed when SiCN was treated at 1300°C with loss of SSA and pore volume. Compared to the SiOC system the SiCN aerogels shows a wider pore size distribution which, for the SiCN-NH_3 samples, goes form few to hundreds nanometers demonstrating a true hierarchical pore structure.

Table 2. Density, SSA and total pore volume values measured for the samples studied.

Sample	SiOC-N_2	SiOC-CO_2	SiOC-NH_3	SiCN-900	SiCN-1300	SiCN-NH_3
Bulk density (g/cm^3)	0.63	0.63	0.61	0.70	0.65	0.45
SSA (m^2/g)	207	314	217	89	30	388
N_2 TPV (cm^3/g)	0.80	0.48	0.84	0.35	0.21	0.61

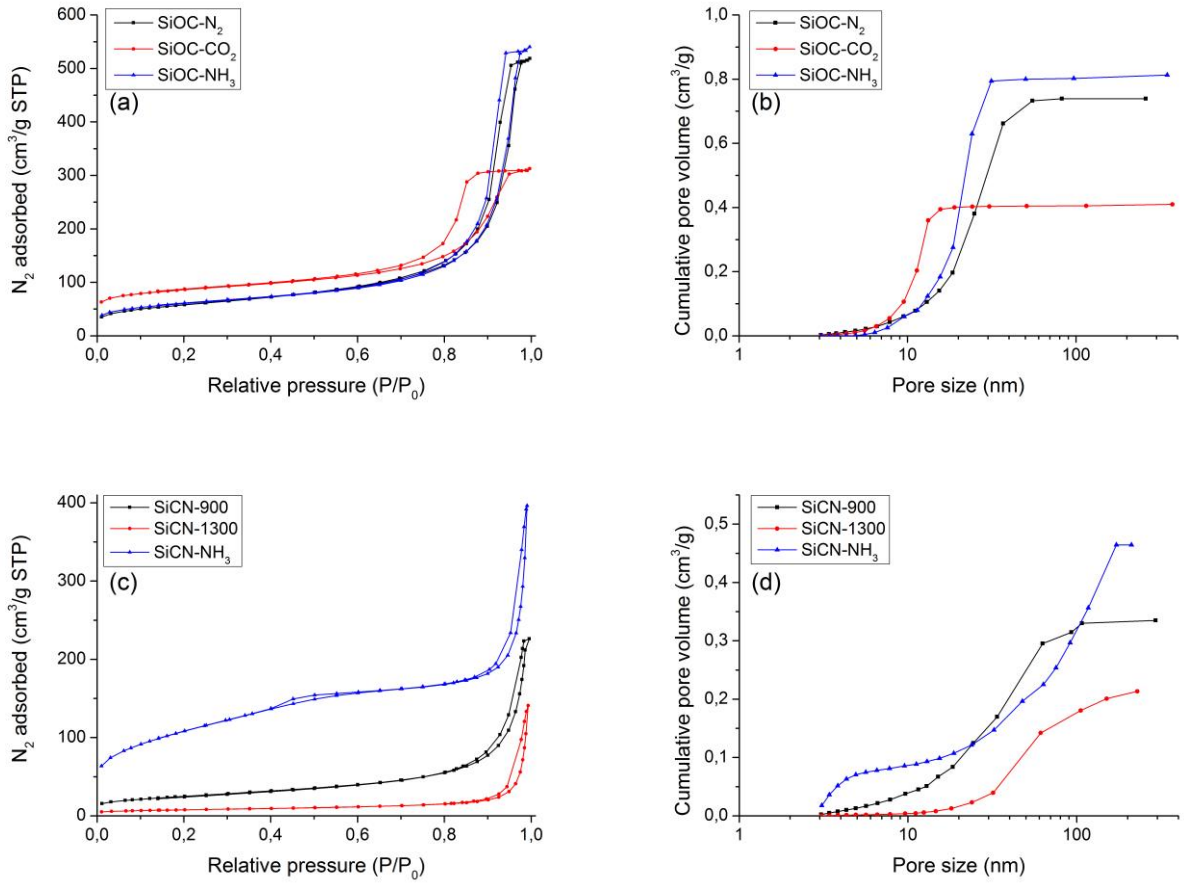

Figure 1. (a), (c) N_2physisorption isotherms and (b), (d) pore size distribution curves of the studied aerogels.

In addition to the microstructure, also the structure, i.e. the type of chemical bonds present in the ceramic aerogels, is modified by the different pyrolysis atmospheres. The chemical bonds present in the aerogels structure were studied recording FT-IR spectra (**Figure 2**). Regarding the polysiloxane-derived SiOC aerogels, the main peaks present in all the spectra are due to Si-O bonds of the amorphous network at 1050 cm^{-1} and 460 cm^{-1} and the C=C bonds of the free carbon phase at 1600 cm^{-1}. The broad peak at 3400 cm^{-1} is related to surface OH groups, with some evidences of isolated Si-OH groups visible as a shoulder at 3600 cm^{-1}. In addition, the presence of C=O bonds at 1700 cm^{-1} is noted for N_2 treated sample and N-H bonds (3160 cm^{-1}) are inserted by the ammonia treatment. The formation of C=O bonds is not yet completely understood since they could be formed during the pyrolythic transformation or, most probably, they could result from the oxidation of the sample after it was exposed to the laboratory atmosphere. Indeed, it has been shown in a previous work that the PDCs aerogels pyrolyzed at low temperature 600-800 °C could be very reactive and they can undergo, after exposure to the laboratory atmosphere, a strong oxidative process with formation of different oxidized species including Si-OH and C=O [27].

The SiCN samples show the presence of the expected Si-N (950 cm^{-1}) and C=C bonds (1600 cm^{-1}), with presence of Si-O (1050 and 450 cm^{-1}) due to the exposure of high SSA polysilazane gels to laboratory atmosphere for rather long time during drying and additional out-of-furnace oxidation effects. Also in this case some -OH groups are present, mostly in the sample treated in NH_3 flow. A strong presence of N-H was observed in the ammonia treated sample. A major difference from the SiOC system is the presence of a peak centered at 1400 cm^{-1}, which was attributed to new C-N bonds [28]. These bonds may be formed during the polymer to ceramic transformation, as already observed pyrolizing a polysiloxane cross-linked

with a silazane in [29], or by insertion of N in the structure by the ammonia treatment (indeed this peak, even if with a much lower intensity, can be recognized also in the spectrum of SiOC NH_3 sample). No clear C=O peaks were ruled out for this set of composition.

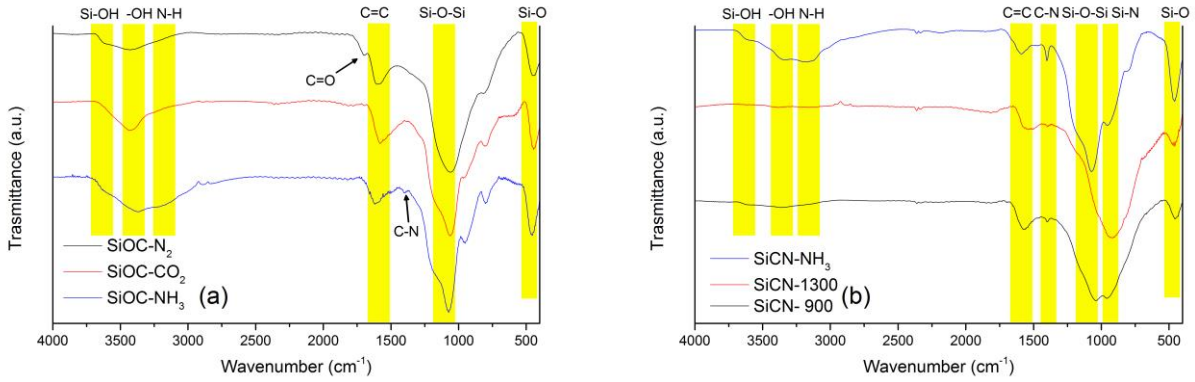

Figure 2. FT-IR spectra of the (a) SiOC and (b) SiCN aerogels.

To investigate more in details the local environment around the silicon atoms of the SiOC samples, ^{29}Si MAS NMR spectra were recorded and are shown in **Figure 3**. The spectra clearly reveal the effect of the 3 different pyrolysis atmospheres on the resulting aerogel structure. In details: pyrolysis under N_2 gives rise to the typical spectrum of silicon oxycarbide glasses with components at -70 and -40ppm assigned, respectively, to $SiCO_3$ and SiC_2O_2 mixed Si sites and at -110 ppm due to SiO_4 silicon units [30]. It is known from the work of Narisawa [12] that pyrolysis of polysiloxanes in CO_2 leads to an amorphous silica network and consumes all the Si-C bonds present in the starting precursor. Accordingly, the ^{29}Si MNR spectrum of the SiOC-CO_2 sample shows only the peak at -110 ppm related to the SiO_4 units. The NMR spectrum of the sample pyrolyzed in ammonia shows two peaks at – 99 and -109 ppm and a shoulder at ~90 ppm. The low field peak can be assigned to SiO_4 units, the one at -99 ppm is related to terminal OH groups present in SiO3(OH) sites while the shoulder at – 90 ppm can be tentatively assigned to silicon atoms sharing bonds with oxygen and nitrogen atoms forming SiO_3N units [31, 32]. The presence of SiO_3N silicon units confirms that pyrolysis under ammonia allows to insert N in the Si-based network. At the same time, peaks in the -40 to-70 ppm range are absent for the SiOC NH_3 sample, suggesting that even in this case Si-C bonds have been cleaved and the amorphous network is now build up only by Si, O and N atoms.

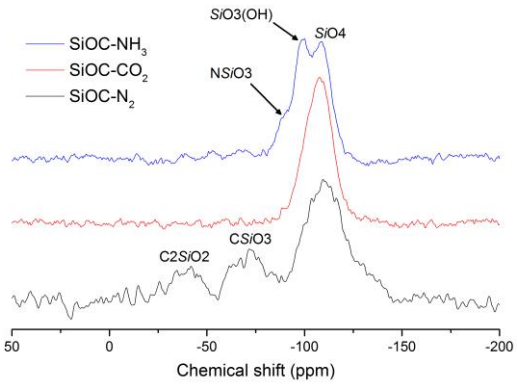

Figure 3. ^{29}Si MAS NMR spectra recorded on the SiOC aerogels pyrolyzed in different atmospheres.

As already described in the introduction, in Si-based polymer derived ceramic a free C phase is usually present. Accordingly, in view of the study of the PDCs aerogels as sorbent materials for Cr ions, the quantitative characterization of the C_{free} phase represents an important information. The quantitative estimation of C_{free} can be done by conventional chemical analysis of Si, O and C and assuming that the fraction of C atoms not bonded to Si atoms forms the free carbon phase [33]. As an alternative, the amount of sp^2 C present in the pyrolyzed materials can be estimated by measuring the weight loss at high temperature in an oxidizing atmosphere (e.g. air), due to the reaction: $C + O_2 \rightarrow CO_2$. This technique gives reliable results only when the oxidation reaction goes to completion. This is not the case when the material is in the form of a bulk sample, however, in the present case, the aerogels are formed by spherical particles with a diameter smaller than 100 nm [34] and the oxidation is supposed to involve the majority of the sample. Thermogravimetric curves measured on the 6 samples are presented in **Figure 4**, and all the curves show a weight loss between 450°C and 800°C allowing to estimate the amount of free carbon (**Table 3**). Interestingly, for the SiCN sample pyrolyzed at 1300°C (SiCN 1300) the oxidation of the free carbon phase is delayed to 600-850°C, due to a lower SSA and a stabilization of the free carbon phase present in the sample induced by the higher pyrolysis temperature.

The samples pyrolyzed in NH_3 show reduced carbon amount, confirming that part of the free carbon was removed during the treatment. A slightly lower amount of carbon was also measured for the SiOC aerogel treated in CO_2. In this case CO_2 can remove part of the free carbon phase through the equilibrium $C + CO_2 \rightarrow 2CO$. The small weight increase observed for samples SiOC N_2, SiCN 900 and SiCN 1300 at temperatures just before the removal of free C is most probably due to the oxidation of C bonded to Si forming Si-C and/or Si-CHx moieties, which leads to a weight increase [35, 25]. It is interesting to note that, for the SiOC aerogel pyrolyzed in CO_2 TGA does not show any weight increase step before the oxidation of free C therefore supporting once more that, for this sample, all the Si-C bonds have been cleaved and transformed into Si-O bonds.

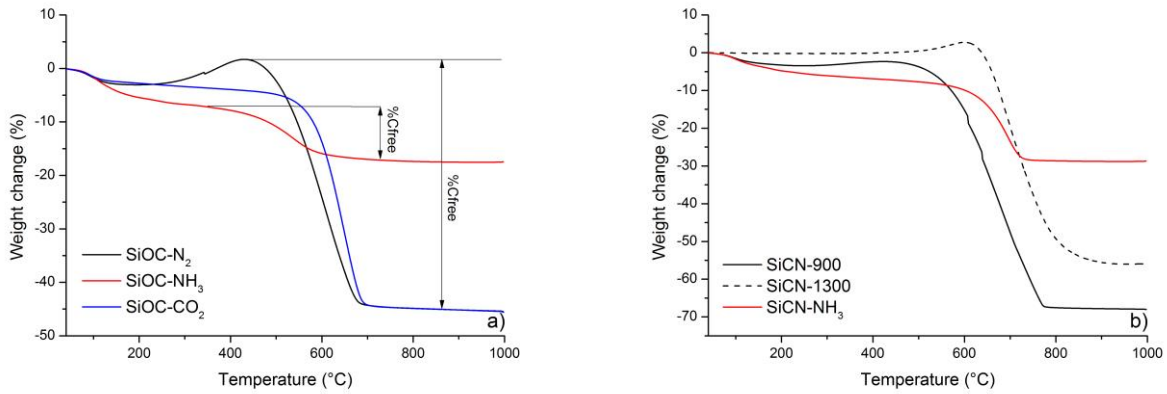

Figure 4. TGA curves recorded in air flow for the (a) SiOC and (b) SiCN aerogels. As an example, in figure 4(a) is show how the Cfree (%) is calculated from the TGA curves.

Table 3. Estimated free carbon content of the studied aerogels.

Sample	SiOC N2	SiOC CO2	SiOC NH3	SiCN 900	SiCN 1300	SiCN NH3
Free C (wt. %)	46	40	12	70	68	25

Some information about the surface acidity/basicity of a material can be inferred by the isoelectric point (IEP). The estimated values are reported in **Table 4**. When N-H bonds are present, the IEP moves toward a more basic value, so ammonia treated samples together with SiCN 900 show more basic surface. When N-H are not present the IEP shifts to lower values, just below 7 for Si-N rich SiCN 1300 and definitely more acidic for Si-O rich SiOCs.

Table 4. Estimated isoelectric points of the studied aerogels.

Sample	SiOC-N_2	SiOC-CO_2	SiOC-NH_3	SiCN-900	SiCN-1300	SiCN-NH3
IEP (pH)	4.89	5.28	9.54	8.91	6.14	9.30

3.2 Cr ion removing tests

With respect to Cr ion adsorption, different behaviors were observed among the six samples tested in buffered pH 5.0 batch conditions (**Figures. 5 & 6**). Cr(VI) ions were effectively removed by SiOC N_2, that exhibits a maximum capacity of 30 mg/g after 1 h (Fig. 5) and SiCN NH_3 samples which adsorbs a maximum of 20 mg/g (Fig. 6), while lower or negligible removal was measured for the other 4 samples. Although a straightforward comparison of the performance of SiOC-N2/SiCN-NH3 sorbents with activated carbons - which are by far the most used adsorbents in the removal of pollutants- is not possible due to different experimental conditions, the above-mentioned capacity values are noteworthy. In fact, a value of adsorption capacity of 3.5 mg/g on activated carbon obtained from sawdust of the coconut tree has been reported by Selvi et al. [36] after 3 hours of contact, while adsorption capacities between 0.6 and 19 mg/g were reported by Enniya et al. [37] for activated carbon obtained from apple peel, after 2 hours of contact. It is noteworthy to mention that the same authors have also measured, for comparison purposes, the adsorption capacity of commercial activated carbon and found a value of 9.5 mg/g. As for the removal of Cr(III), all the aerogels show lower adsorption compared to Cr(VI) and only some of them seem partially effective in removing Cr(III) ions.

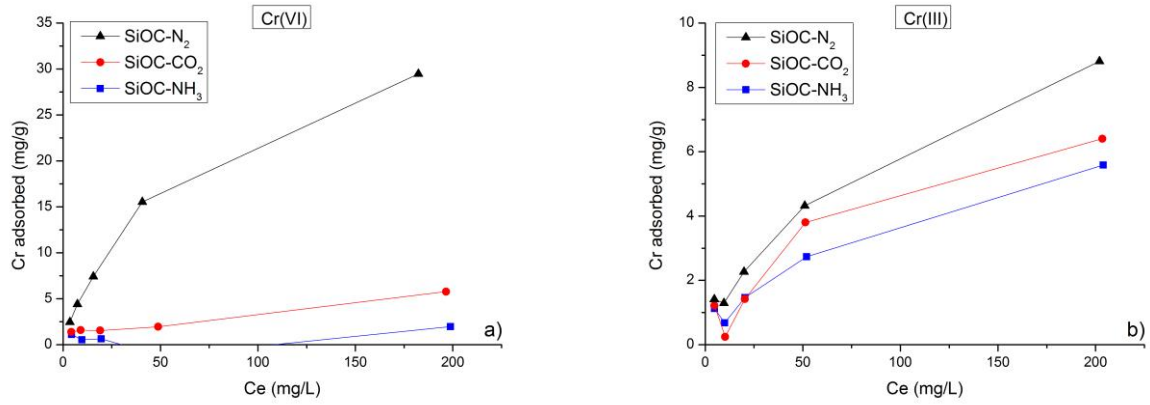

Figure 5. Chromium adsorption isotherms measured for SiOC set using Cr (VI) and Cr(III) ions.

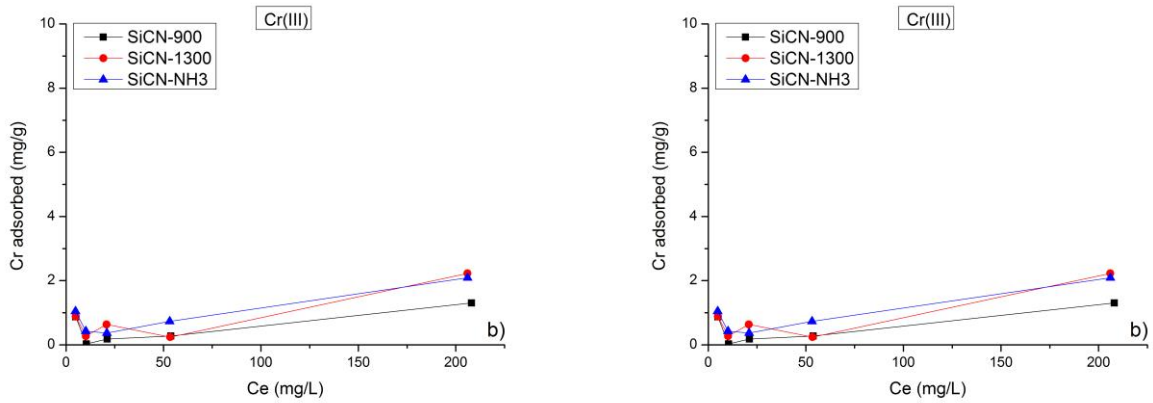

Figure 6. Chromium adsorption isotherms measured for SiCN set using Cr (VI) and Cr(III) ions.

The adsorption of metal ions on a porous material is a very complex process, which can be controlled by several parameters such as the specific surface area, the surface functionalities and the net surface charge, to mention just a few. In our case, the data analysis is even more complicated since the aerogels are not a monophasic materials but indeed they can be regarded as nano-composites consisting in an amorphous Si-based network and a free carbon phase. Accordingly, the relative amount of the two phases could also play a role in controlling the adsorption capacity.

In order to find correlations and similarities among the Cr(VI)/(III) adsorption capacity (Q) with the main features of the porous substrates (SSA, N_2 TPV, amount of free C, bulk density, isoelectric point, main IR peaks (Si-OH, OH, NH, C=O, C=C, Si-O, C-N, Si-N) the Principal Component Analysis (PCA) was applied. PCA is a powerful multivariate technique in which linear combinations of the variables is performed to calculate new variables, called principal components (PC), which are not correlated between themselves. Prior to PCA, data were autoscaled. The scree plot analysis showed that the greatest part of the information (variance) of the original dataset is contained in the first 2 PCs (80%), which were therefore considered for the graphical representation (PC1 *vs* PC2, **Figure 7**). The biplot in Fig. 7 combines the plots of the scores (coordinates of the objects on the new variables PC1 and PC2) and of the loadings (weights of original variables on the linear combination PCs), allowing to recognise groups of samples with similar behaviour and the existing correlation among the original variables.

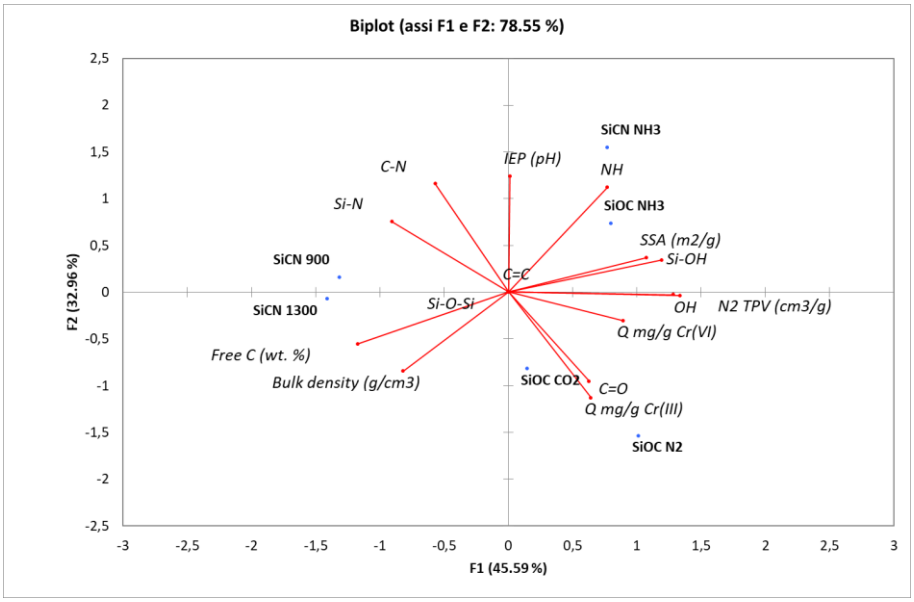

Figure 7. Biplot graph of the objects (each substrate) and of the loadings (red lines: Cr adsorption, bulk density, SSA, N2 TPV, free C, isoelectric point, main IR adsorption bands: Si-OH, OH, NH, C=O, C=C, Si-O, C-N, Si-N).

Concerning the loadings, represented in the plot by the red straight lines, it is possible to see that all variables are almost equally represented on both the principal components, except for IEP which has a significative weight only on PC2. In the biplot graph, variables which appear near to another one are positively correlated, while variables which diagonally opposite each other are negatively correlated. In this respect, adsorption of Cr(VI) appears to be strongly correlated (and therefore positively influenced) both to microstructural parameters such as the SSA and the TPV and to the presence of OH and Si-OH groups. In fact, vectors of SSA, TPV, -OH, Si-OH groups are close to each other and to Q for Cr(VI). Indeed, surface -OH moieties of the materials could interact with oxygen atoms of most frequently found aqueous species of Cr(VI) ($HCrO_4^-$, CrO_4^{2-}, $Cr_2O_7^{2-}$) [38], to create hydrogen bonds.

Differently to what discussed above, vectors related to Si-N and C-N moieties appear diagonally opposed to the vector Q for Cr(III), thus meaning that a strong anticorrelation between these surface functional groups with Cr(III) adsorption is present. This does not necessarily mean that the presence of these groups decreases adsorption of Cr(III), rather than materials characterized by Si-N and C-N groups have negligible interactions with the Cr(III) cation. Same anticorrelated behaviour can be hypothesized for IEP towards Cr(III) adsorption (Q). In this case, it is reasonable to expect that increasing IEP values (leading to a more positive surface) leads to lower adsorption of Cr(III) probably due to electrostatic repulsion between the surface and the Cr cation.

Finally, perpendicular variables have no correlation each other's; this is the case of IEP and Cr(VI) adsorption. Differently from what expected, the increase of IEP (more positive surface) does not directly reflects on a higher adsorption of Cr(VI) anion. In such a case, porosity of the materials seems to control the adsorption, rather than electrostatic interactions. No correlation is observed also for free C and Cr(III)/Cr(VI) adsorption.

The six materials, represented in blue dots, could be divided into three well defined clusters, i. e. SiOC-N_2 and SiOC-CO_2; SiOC-NH_3 and SiCN-NH_3, SiCN-900 and SiCN-1300, according to the values of loadings and scores. Finally if scores and loadings are considered together, it is possible to see the influence of each variable on the different materials. It is therefore easy, and graphically clear, to understand how the material which exhibits higher adsorption performance towards Cr(VI) is SiOC-N2 (as confirmed also in the PC1 vs PC3 biplot graph), while SiOC-N2 has the highest adsorption rates towards Cr(III)

The kinetic curves of the two best performing aerogels for Cr(VI) adsorption, i.e. SiOC-N_2 and SiCN-NH_3, are reported in Figure 8 (a). SiCN-NH_3 aerogels attains the maximum capacity in less than 30 min while the SiOC-N_2 aerogel after 24 h still seems not to have reached its saturation level. The plot of the adsorbed Cr(VI) on the SiOC-N2 substrate as a function square root of time (Figure 8(b)) shows, excluding the last point, a linear correlation suggesting that, for this samples, the kinetics of Cr(VI) adsorption is a diffusion-controlled phenomenon [39, 40]. A similar plot for the SiCN-NH_3 aerogel does not lead to useful information since the kinetics is very fast and we have only two points for the first 30 min, i. e. before reaching the saturation level. However, the much slower kinetics observed for the SiOC-N_2 aerogel compared to the SiCN-NH_3 sample could be explained by the different pore size and pore size distribution of the two materials. SiOC-N_2 displays a less broad and smaller pores (in the range 10 – 30 nm) compared to

the SiCN-NH_3 which shows pores in the range 5 – 200 nm, i. e. a true hierarchical porosity which could allow a much faster ion diffusion toward the adsorbing surface.

Figure 8. (a) Kinetic curves of Cr (VI) adorption for the two best performing aerogels, SiOC-N2 and SiCN-NH3 and (b) plot of the adsorbed Cr(VI) amount on SiOC-N2 as a function of $t^{1/2}$ showing a good linear correlation.

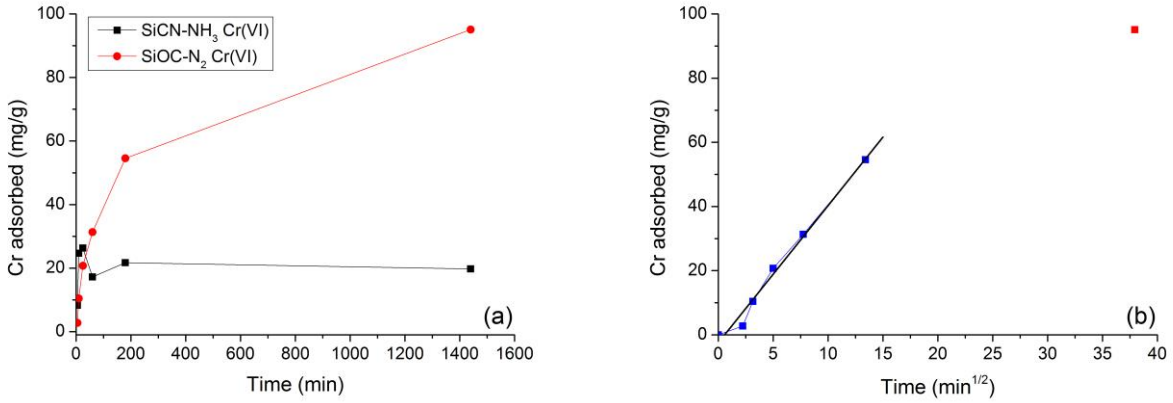

Figure 8. (a) Kinetic curves of Cr (VI) adsorption for the two best performing aerogels, SiOC-N2 and SiCN-NH3 and (b) plot of the adsorbed Cr(VI) amount on SiOC-N2 as a function of $t^{1/2}$ showing a good linear correlation.

Conclusions

Within this work SiOC and SiCN preceramic aerogels were produced from the gelification of a diluted solution containing a polysiloxane or polysilazane and divinylbenzene as crosslinker agent. The open gel structure was maintained thanks to supercritical CO_2 drying for the polysiloxane-based samples while a much simpler evaporative drying was employed for the polysilazane-based ones. The chemical composition of the ceramic aerogels was further manipulated by changing the pyrolysis atmosphere. Accordingly the polysiloxane-derived aerogels have been pyrolyzed in N_2, CO_2 and NH_3 flow while the polysilazane aerogels were pyrolyzed in N_2 and NH_3 flow. As a results 6 different porous SiOC and SiCN ceramic aerogels with a large spectrum of chemical bonds (Si-O, Si-C, Si-N, C=C and C-N), specific surface area, porosity and pore size distribution and surface moieties (Si-OH, OH. N-H and C=O) have been obtained and tested as adsorbents for Cr (III) and Cr(VI) from aqueous solution. It has been found that SiOC and SiCN aerogels pyrolyzed in inert N_2 flow display a good adsorption capacity for Cr(VI) (30 and 20 mg/g respectively after 1 h contact time). Cr (III) can be adsorbed to a lower extent only from the SiOC aerogels while the SiCN aerogels do not show any adsorption capacity, irrespectively from the pyrolysis atmosphere.

Acknowledgements

The authors greatly acknowledge the financial support of “Fondazione Cassa di Risparmio di Trento e Rovereto” under the contract: Polymer-derived ceramics with hierarchical porosity for water filtration/purification (grant number 2015.0174). The authors also acknowledge Mr. Livio Zottele for the ICP measurements and Dr. Emanuela Callone for the NMR measurements.

References

[1] P. Colombo, G. Mera, R. Riedel, G. D. Soraru, *J. Am. Ceram. Soc.* **2010**, *93*, 1805.

[2] F. Dalcanale, J. Grossenbacher, G. Blugan, M. R. Gullo, A. Lauria, J. Brugger, H. Tevaearai, T. Graule, M. Niederberger, J. Kuebler, *J. Europ. Ceram. Soc.* **2014**, *34*, 3559.

[3] S. Dirè. E. Borovin, M. Narisawa, G. D. Sorarù, *J. Mater. Chem. A* **2015**, *3*, 24405.

[4] G. Liu, J. Kaspar, L. M. Reinold, M. Graczyk-Zajac, R. Riedel, *Electrochem. Acta* **2013**, *106*, 101.

[5] L. Zoli, D. Sciti, L.-A. Liew, K. Terauds, S. Azarnoush, R. Raj, *J. Am. Ceram. Soc.* **2016**, *99*, 57.

[6] E. Zanchetta, M. Cattaldo, G. Franchin, M. Schwentenwein, J. Homa, G. Brusatin, P. Colombo, *Advan. Mater.* **2016**, *28*, 370.

[7] D. Assefa, E. Zera, R. Campostrini, G. D. Soraru, C. Vakifahmetoglu, *Ceram, Intern.* **2016**, *42*, 11805.

[8] C. Vakifahmetoglu, D. Zeydanli, M. D. M. Innocentini, F. dos Santos Ribeiro, P. R. Orlandi Lasso, G. D. Soraru, *Sci. Rep.* **2017**, *7*, Article number: 41049.

[9] G. D. Soraru, R. Pena-Alonso, H.-J. Kleebe, *J. Europ. Ceram. Soc.* **2012**, *32*, 1751.

[10] H.-J. Kleebe, G. Gregori, F. Babonneau, Y. D. Blum, D. B. MacQueen, S. Masse, *Int. J. Mater. Res.***2006**, *97*, 699.

[11] V. Belot, R. Corriu, D. Leclercq, P. H. Mutin. A. Vioux, *J. Non-Cryst. Solids* **1992**, *147&148*, 309.

[12] M. Narisawa, F. Funabiki, A. Iwase, F. Wakai, H. Hosono, *J. Am. Ceram. Soc.* **2015**, *98*, 3373.

[13] M.C. Bruzzoniti, O. Abollino, M. Pazzi, L. Rivoira, A. Giacomino, M. Vincenti, *Anal. Bioanal. Chem.* **2017** in press.

[14] F. Fu, Q. Wang, *J. Environ. Manag.* **2011**, *92*, 407.

[15] M. Hua, S. Zhang, B. Pan, W. Zhang, L. Lv, Q. Zhang, *J. Hazard. Mater.* 2012, *211*, 317.

[16] D. Kołodyńska, R. Wnętrzak, J. J. Leahy, M. H. B. Hayes, W. Kwapiński, Z. Hubicki, *Chem. Eng. J.* **2012**, *197*, 295.

[17] M. Hojamberdiev, R. M. Prasad, K. Morita, M. A. Schiavon, R. Riedel, *Microp Mesopor Mater.* **2012**, *151*, 330.

[18] Z. Yua, Y. Feng, S. Li, Y. Pei. *J. Europ. Ceram. Soc.* **2016**, *36*, 3627.

[19] L. Meng, X. Zhang, Y. Tang, K. Su, J. Konget, *Sci Rep.* **2015**, *5*, 7910.

[20] P. Jana, M. C. Bruzzoniti, M. Appendini, L. Rivoira, M. Del Bubba, D. Rossini, L. Ciofi, G. D. Sorarù, *Ceram Intern.* **2016**, *42*, 18937.

[21] M. C. Bruzzoniti, M. Appendini, L. Rivoira, B. Onida, M. Del Bubba, P. Jana, Gi. D. Sorarù, *J. Am. Ceram. Soc,* **2018**, *101*, 821.

[22] D. Zeydanli, S. Akman, C. Vakifahmetoglu, , *J. Am. Ceram. Soc,* **2018**, DOI: 10.1111/jace.15423

[23] G. D. Sorarù, E. Zera, R. Campostrini, (2016). Aerogels from Preceramic Polymers. in Handbook of Sol-Gel Science and Technology, L. Klein et al. (eds.), Springer International Publishing Switzerland 2016,

[24] E. P. Barret, L. G. Joyner, P. P. Halenda, *J. Am. Chem. Soc.* **1951**, *73*, 373.

[25] M. Graczyk-Zajac, D. Vrankovic, P. Waleska, C. Hess, P. Vallachira Sasikumar, S. Lauterbach, H.-J. Kleebe, G. D. Sorarù, *J. Mater. Chem. A* **2018,** *6*, 93.

[26] C. Schitco, M. Seifollahi Bazarjani, R. Riedel, A. Gurlo, *J. Mater. Chem. A* **2015**, *3*, 805.

[27] E. Zera, W. Nickel, S. Kaskel, G. D. Sorarù, *J. Europ. Ceram. Soc.* **2016**, *36*, 423.

[28] G.Socrates, (2004). Infrared and Raman characteristic group frequencies: tables and charts. John Wiley & Sons.

[29] V. L. Nguyen, N. B. Laidani, G. D. Soraru, *J. Mater. Research* **2015**, *30*, 770.

[30] S. J. Widgeon, S. Sen, G. Mera, E. Ionescu, R. Riedel, A. Navrotsky, *Chem. Mater.* **2010**, *22*, 6221.

[31] S. Kohn, W. Hoffbauer, M. Jansen, R. Franke, S. Bender, *J. Non-Cryst. Solids* **1998**, *224*, 232.

[32] F. Hayashi, K. Ishizu, M. Iwamoto, *J. Am. Ceram. Soc.* **2010**, *93* 104.

[33] G. D. Sorarù, G. D'Andrea, R. Campostrini, F. Babonneau, G. Mariotto, *J. Am. Ceram. Soc.* **1995**, *78*, 379.

[34] P. Vallachira Warriam Sasikumar, E. Zera, M. Graczyk‐Zajac, R. Riedel, G. D. Soraru, *J. Am. Ceram. Soc.* **2016**, *99*, 2977.

[35] M. Narisawa, K. Terauds, R. Raj, Y. Kawamoto, T. Matsui, A. Iwase, *Scripta Mater.* **2013**, *69*, 602.

[36] K. Selvi, S. Pattabhi, K. Kirirvelu, *Bioresour. Technol.* **2001**, *80*, 87.

[37] I. Enniya, L. Rghioui, A. Jourani, *Sustainable Chemistry and Pharmacy*, **2018**, *7*, 9

[38] P. Miretzky, A. F. Cirelli, *J. Hazard. Mater.* **2010**, *180*, 1.

[39] V. Fierro, V. Torné-Fernández, D. Montané, A. Celzard, *Micropor. Mesopor. Mater.* **2008**, *111*, 276.

[40] M. C. Bruzzoniti, M. Appendini, B. Onida, M. Castiglioni, M. Del Bubba, L. Vanzetti, P. Jana, G. D. Sorarù, L. Rivoira, *Environ. Sci. Pollut. Res.* **2017**, submitted.